Hindawi
International Transactions on Electrical Energy Systems
Volume 2022, Article ID 2391770, 15 pages
https://doi.org/10.1155/2022/2391770

Research Article

Damping Torque Analysis of the PMSG-Based WT with Supplementary Damping Control for Mitigating Interarea Oscillations

Yanan Yang,[1] **Yujun Li**,[1] **Xiaotian Yuan**,[1,2] **Jiapeng Li**,[1] **and Zhengchun Du**[1]

[1]*School of Electrical Engineering, Xi'an Jiaotong University, Xi'an710000, China*
[2]*School of Electrical and Electronic Engineering, Nanyang Technological University, 639798, Singapore*

Correspondence should be addressed to Yujun Li; yujunlizju@gmail.com

Received 13 June 2022; Revised 5 November 2022; Accepted 14 November 2022; Published 30 November 2022

Academic Editor: N. Prabaharan

This study presents a comprehensive analysis of the impact that a supplementary damping controller of the permanent magnet synchronous generator (PMSG)-based wind turbine (WT) has on low-frequency oscillation (LFO) damping. A reduced mathematical model of an interarea system is first established. Then, an auxiliary damping controller is designed using the PMSG active power control loop, enabling the WT to actively support the interarea LFO mitigation. Based on this, the damping torque analysis (DTA) method is applied to explore the contribution of the PMSG-based WT with an auxiliary damping controller to LFO damping enhancement, whose analytical expressions of the damping torque coefficients reveal the impacts of the control parameters and the operation conditions on the system damping characteristics. It is evident that the installation location of the wind power plant (WPP) plays a leading role in determining whether the damping provided by the PMSG controller is positive or negative. Also, the contribution of damping from the PMSG can be improved by tuning the droop coefficient of the PMSG controller properly. The results indicate that the proposed damping control is always helpful in improving the system damping when the wind power penetration increases. Accordingly, analytical conclusions can serve as guidelines for the control design. Case studies of a two-area test system integrated with a PMSG-based wind farm have been conducted to verify the theoretical analysis.

1. Introduction

Nowadays, the large-scale integration of inverter-connected renewable energy such as wind power has radically changed the structure of the power system and posed significant challenges to the stability of the power system [1–4]. Unlike the synchronous generators (SGs), the wind turbine (WT) does not participate in electromechanical oscillations since the wind power generators are separated from the power grids by the power electronic devices. Thus, high penetration of wind power may affect the inertia [5, 6] and damping characteristics of the power system that used to be dominated by synchronous generators [7–9]. A major concern is the low-frequency oscillation (LFO) problem, especially the interarea oscillations in the interconnected systems, which long exists in the power system and will occur if adequate damping cannot be provided during disturbances [10].

In order to improve the system damping with high penetration of wind power, it has been proposed to equip the WTs with an auxiliary damping control loop to mitigate LFOs [11–17]. Correspondingly, the damping control strategies of variable speed WTs realized by supplementary damping control can be divided into active power modulation [18–21] and reactive power modulation [22–25]. MokhtariAminifar and Li et al. [26, 27] commonly add the auxiliary damping controller to modulate the active power output of the rotor-side converter (RSC) so as to damp the interarea oscillations. Although active power modulation is effective in suppressing electromechanical oscillations, it is found to adversely affect the damping of turbines' shaft

control [28, 29]. Also, the reactive power control of WT is designed to enhance the damping of LFOs. In [23], satisfactory damping can be achieved by equipping the doubly fed induction generator (DFIG) with the proposed power system stabiliser (PSS), which is connected to the reactive power controller of RSC. However, it is reported that the reactive power modulation might deteriorate the voltage stability [20].

Due to the complexity and high order of the power system models, the general approach to verifying the proposed control strategies is based on numerical studies. Modal analysis (MA) is one of the most conventional methods for small-signal stability analysis, which can provide numerical results by analysing the participation patterns of the different system elements. The main advantage of the MA method is that global stability of the system under specified operating conditions can be obtained [30]. The state-space model of a multimachine power system with the DFIG is reported in [10]. It is found that the impact of dynamic interactions introduced by the DFIG increases when wind power penetration increases [31]. In [32], the characteristics of the LFO modes and the dominant states have been comprehensively analysed to study the impact of virtual synchronous machine control on the LFOs. Based on the analysis of the residues of the critical eigenvalues under different conditions, the damping contribution of WTs is evaluated in [33]. To improve the control effects, the power oscillation damper parameters are optimized with the eigenvalue analysis [34]. However, the MA method relies on the numerical results of complicated modal computation, which cannot illustrate why the instability may occur from the physical interpretation. In addition, it fails to formulate a direct mathematical relationship between damping characteristics and influential factors such as the operating point and the parameters of controllers.

To study the mechanism of the impacts of WT on the LFO, the damping torque analysis (DTA) method is employed in [35–43]. Through this method, the electric torque contributed by the controller is decomposed into synchronization torque and damping torque components. The damping torque component determines the damping of the LFOs. For the power system integrated with a DFIG-based wind farm, the effect of the dynamic interactions introduced by the WTs on the oscillation modes is estimated by the DTA method [38]. In [39], the authors provided a very comprehensive examination of the effect of the supplementary HVDC power control on small-signal stability by calculating the damping matrix. The analytical results of [39] were innovatively extended to multiterminal HVDC transmissions in [40]. In [41], the change of load flow and the dynamic interaction introduced by the DFIG are separated to identify the impact of the dynamic interactions of the DFIG with the SGs. Unfortunately, the damping torque coefficients obtained from the above studies are not in analytical form, making it difficult to intuitively evaluate the impacts of the parameters of the WT controller on the LFO mode. In addition, the influencing factors of the LFOs need to be further discussed.

Existing studies primarily focus on the damping effects of LFOs by modulating active or reactive power but rarely care about the mechanism of the supplementary damping controller to deal with LFOs. This study develops insights into the contribution of the PMSG-based WT with an auxiliary damping controller to LFO mitigation by the DTA method. Firstly, this study developed a dynamic reduced model of an interarea system oriented to the small-signal stability analysis. Then, an auxiliary damping control strategy for the PMSG-based WT is designed by the droop control loop, which uses the rotational speed signal between generators to guide the active power modulation. Based on this, the DTA method is applied to evaluate the contribution of WT control on LFO mitigation, whose explicit expressions of the damping torque coefficients are analytically derived. Consequently, qualitative evaluations of the operation conditions and the control parameters on the system damping characteristics can be achieved, providing useful guidance for the controller design.

The rest of this study is organized as follows. Section 2 constructs a reduced dynamic model of an interarea system. In Section 3, an auxiliary damping control based on a droop control scheme is proposed to restrain the LFOs of the PMSG-based WT. Section 4 applies the DTA method to obtain some analytical conclusions. The analytical results are verified by simulations in Section 5. Section 6 summarizes the main conclusions of this study.

2. Modelling of the Interarea System

As a mainstream type of variable speed wind turbine, the PMSG-based WT is widely used due to its excellent control features. In this section, a simplified dynamic model of a two-area system integrated with a PMSG-based wind farm is first established. Then, the mathematical model and conventional control scheme of the PMSG are briefly introduced.

2.1. A Reduced Dynamic Model of the Interarea System. As shown in Figure 1, an interarea system integrated with the PMSG-based wind power plant (WPP) is first constructed. For simplification, the AC grid of each area is modelled as the equivalent generators SG_1 and SG_2. Hence, the dynamics of the AC grids can be represented by two synchronous generators. The AC transmission lines of the studied system are regarded as lossless and without energy storage.

As for generators, the classical machine model is adopted, with a stiff electromotive force behind a transient reactance. Under the consideration of eliminating the damping effect of the SGs, the damping windings of SG_1 and SG_2 (including the damping effect caused by eddy currents in the rotor core) are neglected, and the damping coefficient values of SG_1 and SG_2 are regarded as zero ($D_1 = D_2 = 0$).

The swing equations of SG_1 and SG_2 can be written as follows:

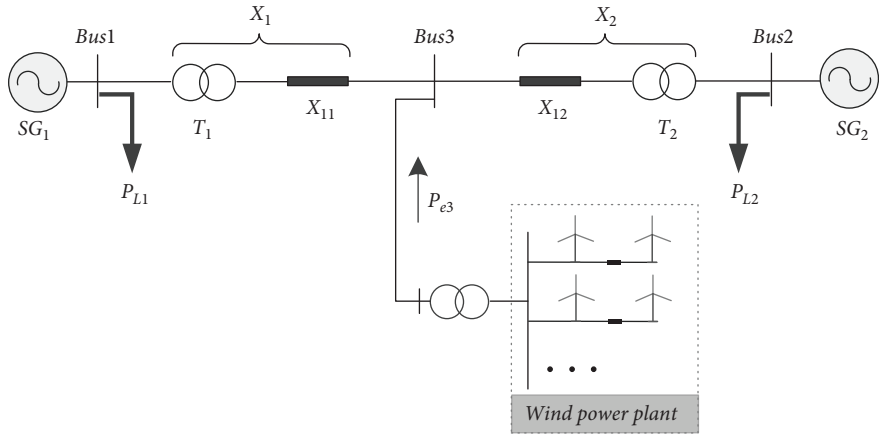

Figure 1: Structure of an interarea system.

$$\begin{cases} 2H_1\dfrac{d\omega_1}{dt} = P_{M1} - P_{e1} - P_{L1}, \\ 2H_2\dfrac{d\omega_2}{dt} = P_{M2} - P_{e2} - P_{L2}, \\ \dfrac{d\delta_1}{dt} = \omega_s(\omega_1 - 1), \\ \dfrac{d\delta_2}{dt} = \omega_s(\omega_2 - 1), \end{cases} \tag{1}$$

where H_1 and H_2 are the inertia constants, P_{M1} and P_{M2} are the mechanical power inputs of generators SG_1 and SG_2, respectively, P_{e1} and P_{e2} are the active power outputs of generators SG_1 and SG_2, respectively, P_{L1} and P_{L2} are the local loads, ω_1, ω_2 and δ_1, δ_2 are the rotor speed and rotor angle of SG_1 and SG_2, respectively, and ω_s is the synchronous electrical angular velocity. The mathematical model mentioned in (1) is the simplest dynamic representation of a synchronous generator. Based on this, it is possible to decouple the damping effect introduced by WT from the power system.

Active power balances at Bus 3 add the relation

$$\frac{V_1V_3}{X_1}\sin(\delta_1 - \delta_3) + \frac{V_2V_3}{X_2}\sin(\delta_2 - \delta_3) + P_{e3} = 0, \tag{2}$$

where X_1 and X_2 are the total reactance of the transmission line in each area, as shown in Figure 1, δ_3 is the voltage phase at Bus 3, and P_{e3} is the active power output from the WPP. In normal operation, the voltage magnitudes of all busbars vary within a small range because of the regulation of the excitation system and the injected reactive power. For this reason, it is assumed that the voltage magnitudes of all busbars are equal, which meets the condition that $V_1 = V_2 = V_3 = V$. Under this assumption, the linearization equation (2)becomes

$$\frac{V^2}{X_1}\cos(\delta_{1(0)} - \delta_{3(0)})\cdot(\Delta\delta_1 - \Delta\delta_3) + \frac{V^2}{X_2}\cos(\delta_{2(0)} - \delta_{3(0)})\cdot(\Delta\delta_2 - \Delta\delta_3) + \Delta P_{e3} = 0, \tag{3}$$

where the prefix "Δ" is the incremental operator that denotes the small deviation of a variable. The subscript (0) of each variable represents its steady-state value. For simplification, the variables a_1 and a_2 are defined as follows:

$$\begin{cases} a_1 = \dfrac{V^2}{X_1}\cos(\delta_{1(0)} - \delta_{3(0)}), \\ a_2 = \dfrac{V^2}{X_2}\cos(\delta_{2(0)} - \delta_{3(0)}). \end{cases} \tag{4}$$

Then, $\Delta\delta_3$ can be solved based on (3) and (4):

$$\Delta\delta_3 = \frac{a_1}{a_1 + a_2}\Delta\delta_1 + \frac{a_2}{a_1 + a_2}\Delta\delta_2 + \frac{\Delta P_{e3}}{a_1 + a_2}. \tag{5}$$

Substituting (3) and (4) into the small-signal dynamic model of (1), the simplified dynamic equations of the interarea system can be obtained as follows:

$$\begin{cases} 2H_1H_2\dfrac{d\Delta\omega}{dt} = -\dfrac{a_1a_2(H_1 + H_2)}{a_1 + a_2}\Delta\delta + \dfrac{H_2a_1 - H_1a_2}{a_1 + a_2}\Delta P_{e3}, \\ \dfrac{d\Delta\delta}{dt} = \omega_s\Delta\omega, \end{cases} \tag{6}$$

where

$$\begin{cases} \Delta\omega = \Delta\omega_1 - \Delta\omega_2, \\ \Delta\delta = \Delta\delta_1 - \Delta\delta_2, \end{cases} \tag{7}$$

where $\Delta\omega$ is the rotational speed deviation between SG_1 and SG_2 and $\Delta\delta$ is the rotor angle deviation between SG_1 and SG_2. If the active power output from the WPP is zero (i.e., $P_{e3} = 0$) in (6), then Bus 3 can be considered a point to observe the voltage phase along the line since it has no impact on the system dynamics. In this case, the Laplace transform of (6) can be expressed as

$$\frac{2H_1H_2}{\omega_s}s^2 + \frac{a_1a_2\left(H_1 + H_2\right)}{a_1 + a_2} = 0. \tag{8}$$

Then, the undamped natural mechanical mode frequency can be solved as follows:

$$s_{1,2} = \pm j\omega_n, \omega_n = \sqrt{\frac{\omega_s a_1 a_2 \cdot \left(H_1 + H_2\right)}{2\left(a_1 + a_2\right) \cdot H_1H_2}}. \tag{9}$$

As shown in (6), the dynamic behaviour of a two-area model can be similarly represented by an equivalent single-machine infinite-bus (SMIB) model. However, if the full mode of the two-area system is considered, the relative degree will be large. Thus, the design of the WT damping controller will use a high-order derivation, which will be much more difficult. Otherwise, the reduced dynamic mathematical model in (6) has many advantages. (i) Firstly, the complexity of the interarea system model has been greatly reduced since the model has been reduced from fourth order to second order. (ii) Secondly, the initial parameters of two interconnected synchronous generators are retained in (6) after some simple formula reconstructions and variable substitutions. (iii) Finally, the effect of the injected power at Bus 3 on LFOs is clearly outlined in (6), allowing the derivation of the equivalent damping torque provided by the WT controller. For these reasons, the electromechanical dynamics of the interarea system in (1) can be represented by the dynamic equations in (6).

2.2. PMSG-WT with the Conventional Control Scheme. As shown in Figure 2, the conventional controller of PMSG is composed of a rotor-side converter (RSC) and a grid-side converter (GSC). In this study, the RSC controls the PMSG generated active power, while the GSC is utilized to maintain the DC-link voltage. Normally, the active power generated by the PMSG is controlled through the maximum power point tracking (MPPT) algorithm and the pitch angle control.

The output power of the PMSG under the MPPT control can be expressed as

$$P_{MPPT} = \frac{\rho\pi R^5 k^3 C_{p\max}}{2\lambda^3} \cdot \omega_t^3 = C_M \cdot \omega_t^3, \tag{10}$$

where ρ is the air density, R is the rotor blade radius, k is the gear ratio of the gearbox, λ is the tip speed ratio, C_p is the maximum power coefficient as λ takes a certain value, and ω_t is the PMSG generator rotational speed.

Generally, the control scheme at the back-to-back VSCs of a PMSG primarily includes the inner current control loop and the outer control loop. Due to the fast response of the double loop controller system, the converter dynamics of the PMSG can be overlooked. Therefore, the generated active power P_{WT} can be regarded as the same as its power reference, which is determined by the MPPT algorithm P_{MPPT}. Under the assumption that the converter is lossless, the equation for the PMSG output power is given by

$$P_{e3} = P_{WT}. \tag{11}$$

The rotor motion dynamic equation of the PMSG can be described as

$$2H_t \cdot \omega_t \cdot \frac{d\omega_t}{dt} = P_{\text{wind}} - P_{WT}, \tag{12}$$

where H_t is the inertia time constant of the PMSG.

3. Proposed Damping Controller by Droop Control

This section proposes a droop control strategy for the PMSG to provide additional damping for the interarea system. For the conventional PMSG control strategy, the PMSG output power is completely handled by the fast converter control. However, this converter control strategy decoupled the rotational speed of the PMSG from the grid frequency. Consequently, the PMSG cannot provide damping after a disturbance, which might diminish the ability of damping LFOs in the power system.

In order to improve the damping of the WT, most existing studies focus on implementing the interarea oscillation damping control via auxiliary droop control. The output of the droop control loop can be expressed as

$$\Delta P_{\text{droop}} = -K_{WT}\left(\omega_{\text{sys}} - \omega_{\text{nom}}\right), \tag{13}$$

where ω_{sys} is the system rotational speed in p.u., ω_{nom} is the nominal rotational speed in p.u., and K_{WT} is the droop coefficient. The principle of this auxiliary damping control can be explained as follows. Once the system is disturbed; for example, a sudden load increase occurs in the power system. Then, the rotational speed of the system will deviate from its nominal rotational speed, which activates the droop control loop in (13) and adds a power component related to the rotational speed to the PMSG reference power. Subsequently, the turbine slows down and releases kinetic energy from the rotor to modulate the imbalanced power in the power system.

In this study, an auxiliary damping control using the signal of the rotational speed deviation between SG_1 and SG_2 has been particularly developed. There are several considerations for using $\Delta\omega$ as the input signal. Firstly, $\Delta\omega$ is in accordance with the reduced dynamic model of the interarea system derived in (6), which might simplify the design of auxiliary damping control. Additionally, the input signal $\Delta\omega$ can automatically detect the speed deviation between generators, which might provide damping more effectively. Also, damping the LFOs is meant to keep the relative angle

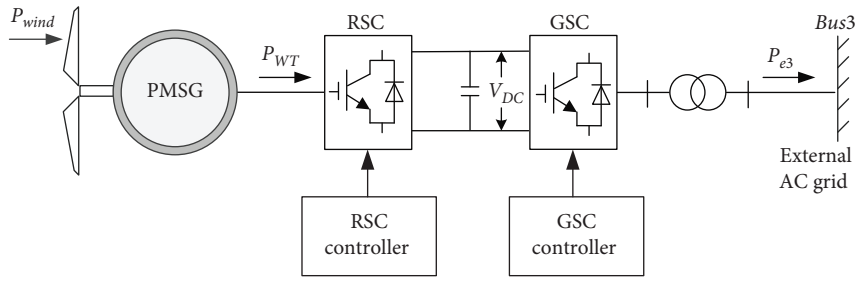

Figure 2: The configuration of a PMSG connecting to a large system.

between the two areas as a constant. In other words, it is to maintain the rotational speed deviation $\Delta\omega$ at a value of zero.

Accordingly, the reference power of PMSG can be written as

$$P_{WT} = P_{MPPT} - K_{WT}\Delta\omega. \tag{14}$$

For the steady state, the relative rotor speed $\Delta\omega$ and the active power for damping control ΔP_{droop} are both zeros. Figure 3 displays the structure of the PMSG droop control. In Figure 3, ΔP_{droop} is limited to 0.1 p.u. to ensure that the current of the IGBTs in the converter does not exceed its limits. As for the proposed droop control scheme in Figure 3, the signal of the rotational speed deviation $\Delta\omega$ is sent through a deadband filter first, which is used to avoid the reaction of the controller to very small rotational speed variations during normal operation. Considering small disturbances of the rotational speed, it is necessary to set the threshold value of the rotational speed deviation $\Delta\omega$, which is the input signal of the droop control. In this study, the threshold value of the rotational speed deviation is set as $\Delta\omega = \pm 0.02$ p.u. in the deadband filter.

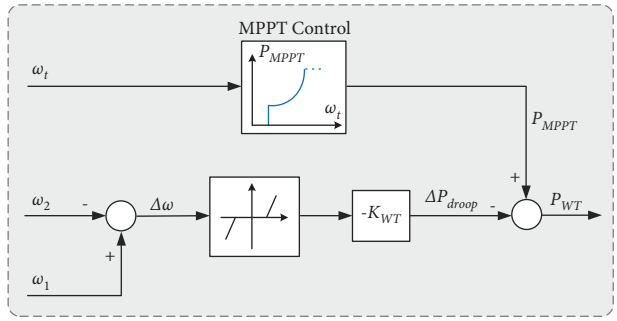

Figure 3: Structure of the PMSG droop control.

4. Low-Frequency Oscillation Analysis of PMSG Integrated Power System

The DTA is a conventional and effective method to evaluate the ability to damp oscillations. In this section, the DTA method is applied to clearly outline the effect of the auxiliary damping control of PMSG on the LFOs. Moreover, the damping torque provided by the PMSG controller is explicitly derived for further analysis.

4.1. Dynamic Model of the Studied System. Considering the structure of a WPP integrated into the interarea power system in Figure 1, some assumptions need to be made. (i) Firstly, the impact of the automatic voltage regulator (AVR) and the power system switch (PSS) on the power system dynamics are overlooked. (ii) Secondly, it is assumed that the deviation of voltage-angle between busbars is comparatively small in this study. (iii) Finally, it is supposed that the rotor speed signal of the synchronous generator can be transmitted to the wind turbine terminals through wide area control systems (WACS) instantaneously, i.e., the communication delay can be neglected.

Suppose that the wind speed remains constant during a comparatively short period; then, the linearized model of the PMSG equipped with auxiliary damping control (cf. Section 3) can be established as follows:

$$\begin{cases} 2H_t \cdot \omega_{t(0)} \cdot \dfrac{\mathrm{d}\Delta\omega_t}{\mathrm{d}t} = -\Delta P_{e3}, \\ \Delta P_{e3} = 3C_M\omega_{t(0)}^2\Delta\omega_t - K_{WT}\Delta\omega. \end{cases} \tag{15}$$

Combining (15) with (6) and using the Laplace transformation yield

$$2H_1H_2\frac{\mathrm{d}\Delta\omega}{\mathrm{d}t} = -\frac{a_1a_2(H_1+H_2)}{a_1+a_2}\Delta\delta - \underbrace{\frac{H_2a_1 - H_1a_2}{a_1+a_2}\frac{2H_t\omega_{t(0)}K_{WT}s}{3C_M\omega_{t(0)}^2 + 2H_t\omega_{t(0)}s}}_{F(s)}\Delta\omega. \tag{16}$$

The last term of (16), $F(s)$, is an electrical torque, which contributes to the auxiliary damping control of the PMSG-based WT. According to the classical DTA method, the electrical torque component can be decomposed into the synchronizing and damping components, which are in phase with the rotor angle perturbation and the angle speed

deviation, respectively. Since the system damping torque coefficient is comparably small to the synchronizing torque coefficient, the system oscillation frequency can be represented by the natural oscillation frequency in (9). Accordingly, (16) can be reformulated as

$$T_J \frac{\mathrm{d}\Delta\omega}{\mathrm{d}t} = -K_S \Delta\delta - K_D \Delta\omega, \tag{17}$$

where

$$\begin{cases} K_S = \dfrac{a_1 a_2 (H_1 + H_2)}{a_1 + a_2}, \\ K_D = \dfrac{H_2 a_1 - H_1 a_2}{a_1 + a_2} \dfrac{4H_t^2 K_{WT} \omega_n^2}{\left(3C_M \omega_{t(0)}\right)^2 + \left(2H_t \omega_n\right)^2}, \\ T_J = 2H_1 H_2 + \dfrac{H_2 a_1 - H_1 a_2}{a_1 + a_2} \dfrac{6C_M H_t K_{WT} \omega_{t(0)}}{\left(3C_M \omega_{t(0)}\right)^2 + \left(2H_t \omega_n\right)^2}, \end{cases} \tag{18}$$

where T_J is the equivalent inertia constant provided by the synchronous generator and the PMSG, K_S is the synchronizing torque coefficient, and K_D is the damping torque coefficient.

4.2. Damping Torque Analysis. According to (18), the damping torque coefficient of the studied system is correlated with the parameters of the PMSG damping control. Due to the small variation between generators, the cosine function $\cos(\delta_{i(0)} - \delta_{j(0)})$ in (18) can be approximated as 1. Then, the damping torque coefficient can be obtained as

$$K_D = \frac{H_2 X_2 - H_1 X_1}{X_1 + X_2} \frac{4H_t^2 K_{WT} \omega_n^2}{\left(3C_M \omega_{t(0)}\right)^2 + \left(2H_t \omega_n\right)^2}. \tag{19}$$

In (19), the equivalent damping torque coefficient is not only related to the droop control coefficient K_{WT} but also affected by the installed location of the WPP. The damping torque analysis will be conducted in the following section to clearly outline the effect of these factors.

4.2.1. The Impact of the Location of the WPP. From (19), it can be seen that the relative location of the WPP to the two SGs affects the damping level of the studied system. The line reactance from the WPP to SG_1 and SG_2 are noted as X_{l1} and X_{l2}, respectively. Assuming that the reactance of the transmission line is well distributed, then the WPP location can be expressed by the relative distance from SG_1 noted as l_w:

$$\begin{cases} X_{l1} = l_w X, \\ X_{l2} = (1 - l_w) X, \end{cases} \tag{20}$$

where X is the total reactance of the transmission line 1 and the transmission line 2.

If the WPP is located at the mass-weighted electrical centre between the two areas, i.e., $H_2X_2 = H_1X_1$, then the damping torque coefficient K_D will reduce to zero. In this case, the PMSG damping control has no impact on the interarea LFOs, and consequently, the WT injected power has no contribution to the LFOs' damping. The location of the mass-weighted electrical centre can be expressed by l_w:

$$l_w = \frac{H_2 (X_{T2} + X) - H_1 X_{T1}}{(H_1 + H_2) X}, \tag{21}$$

where X_{T1} and X_{T2} are the reactance of transformers T_1 and T_2. Obviously, the interarea mode is uncontrollable by using the PMSG auxiliary damping control as long as the WPP is located at the mass-weighted electrical centre.

Area 1: if the WPP is installed between the mass-weighted electrical centre and SG_1, i.e., $H_1X_1 < H_2X_2$, then the WPP is relatively close to SG_1 in the electrical distance. The range of this area can be expressed by l_w:

$$0 < l_w < \frac{H_2 (X_{T2} + X) - H_1 X_{T1}}{(H_1 + H_2) X}. \tag{22}$$

In this case, the damping torque coefficient K_D is positive. Therefore, the damping control of PMSG has a positive contribution to LFO damping. Moreover, the closer the WPP is to SG_1 (see Figure 1), the higher the damping torque coefficient K_D is. Especially, the PMSG controller gives the largest contribution to the oscillation damping when the WPP terminal is located near the centre of SG_1, and the maximal damping torque coefficient is

$$K_D = \frac{4H_2 H_t^2 K_{WT} \omega_n^2}{\left(3C_M \omega_{t(0)}\right)^2 + \left(2H_t \omega_n\right)^2}. \tag{23}$$

Area 2: similarly, if the WPP is installed between the mass-weighted electrical centre and SG_2, i.e., $H_1X_1 > H_2X_2$, then the WPP is relatively close to SG_2 in the electrical distance. The restriction of l_w can be derived as

$$\frac{H_2 (X_{T2} + X) - H_1 X_{T1}}{(H_1 + H_2) X} < l_w < 1. \tag{24}$$

As seen in (19), if $H_1X_1 > H_2X_2$, then $K_D < 0$. The PMSG damping control gives a negative contribution to the LFO damping. One may also notice that the PMSG controller placed closer to the generator SG_2 (as shown in Figure 1) has a higher impact on the damping torque coefficient. The negative damping torque coefficient K_D is maximized as the WPP is installed near SG_2, giving

$$K_D = -\frac{4H_1 H_t^2 K_{WT} \omega_n^2}{\left(3C_M \omega_{t(0)}\right)^2 + \left(2H_t \omega_n\right)^2}. \tag{25}$$

It can be concluded that the PMSG auxiliary damping control will provide a positive damping torque to the system when the WPP is installed in Area 1. Otherwise, a negative damping torque will be obtained when the WPP is installed in Area 2. One may notice that the WPP placed closer to SG_1 has a better damping effect on the LFOs.

4.2.2. The Impact of K_{WT}. The sensitivity of the damping torque coefficient K_D to the droop coefficient K_{WT} is given by

$$\frac{\partial K_D}{\partial K_{\mathrm{WT}}} = \frac{H_1 X_1 - H_2 X_2}{X_1 + X_2} \frac{4H_t^2 \omega_n^2}{\left(3C_M \omega_{t(0)}\right)^2 + \left(2H_t \omega_n\right)^2}. \quad (26)$$

Equation (26) shows the analytical relationship between the droop coefficient of the PMSG damping control and the change in damping torque coefficient. Considering the case that the WPP is located in Area 1, then the damping torque coefficient K_D is positive, and its value increases with the increase in the droop coefficient K_{WT}. In this case, the damping provision of the WT can be enhanced by increasing K_{WT}. The higher K_{WT}, the stronger the damping effect of the WT controller on the LFO. Moreover, the sensitivity of K_D to K_{WT} is affected by the location of the WPP. It can be seen from (26) that K_D is more sensitive to K_{WT} if the WPP is placed closer to SG_1.

On the contrary, if the WPP is located in Area 2, the WT controller will exhibit negative damping on system oscillation, and the value of K_D decreases as K_{WT} increases. In this case, a higher droop coefficient will deteriorate the damping level and aggravate the LFO. To sum up, the installation location of the WPP plays a leading role in determining whether the damping provided by the WT controller is positive or negative, and even more, the damping of the interarea oscillations can be improved by turning the droop coefficient. However, the effectiveness of the WT damping control is also affected by the installation location of the WPP, with modulation being more efficient when the WPP is close to SG_1.

5. Simulation Studies

To demonstrate and evaluate the proposed control scheme, a simple simulation system consisting of two synchronous generators (SG_1 and SG_2), a PMSG-based wind plant, and two local loads (P_{L1} and P_{L2}) described in Figure 1 is modelled. A WPP consisting of 196 (14×14) units of PMSG is modelled, as well as the rating of each WT converter is set the same as 2 MW. The rated capacity of SG is 300 MW and the wind power capacity penetration level in this study is around 30%. All variables are expressed in per-unit (p.u.) quantities for the test system. More parameters of the test system is in Tables S1 and S2 in the Supplementary Material. In this study, the simulation is developed on the MATLAB platform.

5.1. Impact of the WPP Installation Location. In this case, the impact of the WPP location was analysed by changing the reactance of the interconnection lines X_{l1} and X_{l2} in Figure 1. The gain of the droop loop K_{WT} is set to 10. Figure 4 shows the eigenvalue trajectories with l_w (the relative distance from SG_1) increasing from 0 to 1, as well as the WPP installation location moving along the transmission line and close to SG_2. It can be seen that, with l_w increasing from 0 to 1, the dominant mode $\lambda_{1,2}$ moves from the left half of the complex plane to the right, and K_D varies from 13.41 to −32.76.

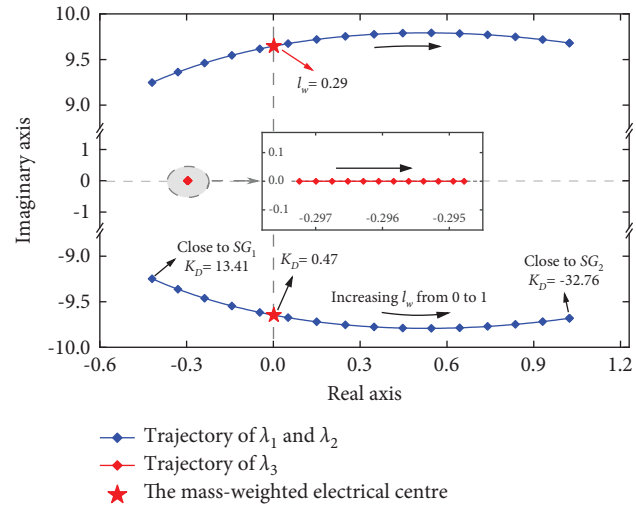

Figure 4: Eigenvalue trajectories with l_w increasing from 0 to 1.

Furthermore, it is interesting to find that there is a critical stable point in the imaginary axis when $l_w = 0.29$, which is indeed the mass-weighted electrical canter. Thus, it can be concluded that the WPP placed close to SG_1 might increase the stability of the studied system, which also verifies the accuracy of the damping torque analysis in Section 4.2.

To illustrate the impact of the WPP installation location in detail, two different cases, including the curves in the right and left halves of the complex plane in Figure 4, which correspond to Area 1 and Area 2, are considered, respectively. Table 1 shows the interarea oscillation mode $\lambda_{1,2}$ when the WPP is located in Area 1. Apparently, as the WPP is placed closer to the mass-weighted electrical centre within Area 1, the damping ratio is decreasing and approaching zero. It can also be seen that mode $\lambda_{1,2}$ dominates the LFO with a frequency of approximately 1.5 Hz. Furthermore, the confirmation of simulations corresponding to Table 1 is presented in Figure 5. Assuming that a sudden load event occurs at Bus 1, the load P_{L1} increases 0.1 p.u. at $t = 1$ s. As displayed in Figure 5, the oscillations of Location B (l_w = 0.167) are damped better than those of Location A (l_w = 0), confirming the correctness of the results obtained in Figure 4. In particular, the dark curve represents that the contribution to system damping is zero when the WPP is located at the mass-weighted electrical centre, which is consistent with the analysis made by (19).

Similarly, the oscillation mode of the example system that the WPP is installed in Area 2 is listed in Table 2. One may also notice that the WPP placed closer to SG_2 has a negative impact on the damping torque coefficient K_D. To illustrate this, the time-domain responses for Location C (l_w = 0.333) and Location D (l_w = 0.388) are visualized in Figure 6. It is indicated that, with l_w varying from 0.289 to 0.389, the installation location of the WPP is placed closer to SG_2 and the risk of oscillatory instability is increasing. In summary, the installation location of the WPP significantly affects the system damping in the concerned oscillation mode. Based on the results, it is clear that the impact of the PMSG auxiliary controller on LFO damping can be positive

Table 1: Comparison of different installation locations of the WPP in area 1. ($K_{WT}=10$, wind energy ratio of 30%).

Location	Location A	Location B	The mass-weighted electrical centre
X_{l1} (p.u.)	0.15	0.3	0.41
l_w	0	0.167	0.289
Damping ratio	0.0453	0.0201	0.0015
K_D	13.41	6.12	0.47
Oscillation frequency (Hz)	1.47	1.51	1.53
Eigenvalue	$-0.42 \pm 9.25j$	$-0.19 \pm 9.51j$	$-0.01 \pm 9.64j$

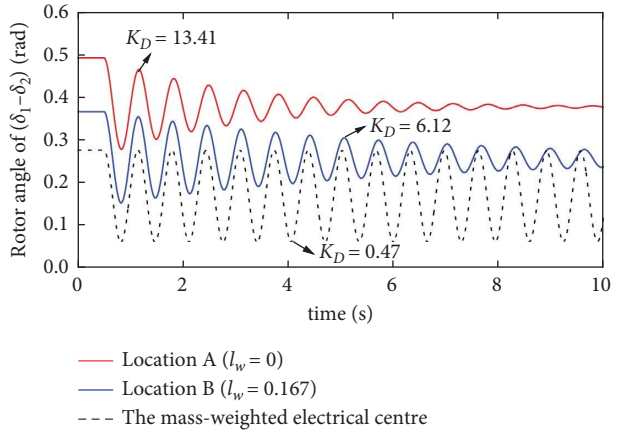

Figure 5: Simulation results of different locations in area 1.

Table 2: Comparison of different installation locations of the WPP in area 2. ($K_{WT}=10$, wind energy ratio of 30%).

Location	The mass-weighted electrical centre	Location C	Location D
X_{l1} (p.u.)	0.41	0.45	0.5
l_w	0.289	0.333	0.389
Damping ratio	0.0015	−0.0052	−0.0137
K_D	0.47	−1.62	−4.254
Oscillation frequency (Hz)	1.53	1.54	1.55
Eigenvalue	$-0.01 \pm 9.64j$	$0.05 \pm 9.67j$	$0.13 \pm 9.71j$

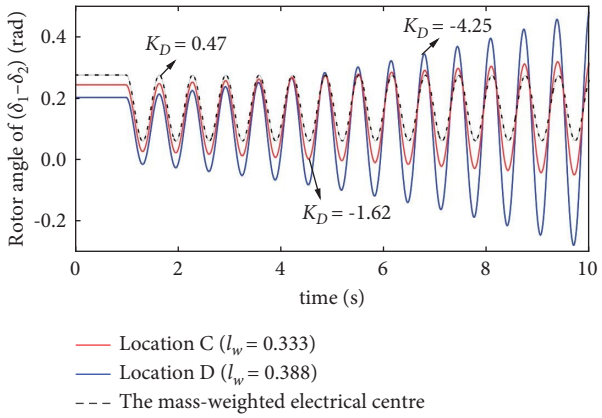

Figure 6: Simulation results of different locations in area 2.

or negative, depending on the WPP location. The simulation results and the eigenvalue analysis are fully consistent with the damping torque analysis.

5.2. Impact of the Droop Coefficient. In this section, test results are presented to evaluate the impact of the droop coefficient K_{WT} of the PMSG auxiliary damping control on

LFOs. As shown in Figure 7, the eigenvalue trajectory results are depicted when the WPP is located at Location B in the stable region and Location C in the unstable region, respectively. Figure 7(a) shows the eigenvalue trajectories when the WPP is placed at Location B (in Area 1) as the droop coefficient K_{WT} varies from 1 to 100. With the increase of K_{WT}, the dominant mode $\lambda_{1,2}$ moves leftward in the plane, and the damping torque coefficient increases from 2.45 to 61.16. However, if the WPP is placed at Location C (in Area 2), the dominant mode $\lambda_{1,2}$ lies in the right half of the complex plane, as shown in Figure 7(b). In this case, a higher droop coefficient K_{WT} will deteriorate the modal damping, and thus, the PMSG auxiliary damping control plays a negative role in damping the LFOs. The analytical results derived from equation (26)agree with the results mentioned above.

To better show the effect of the PMSG controller on the LFOs, assuming that a sudden load increase of 10% occurs in P_{L1} at $t = 1$ s, the simulation results with different droop coefficients K_{WT} are shown in Figure 8. Figure 8(a) shows the time-domain responses of the power angle deviation between SG_1 and SG_2 with $K_{WT} = 10$ and $K_{WT} = 20$ when the WPP is placed at Location B. In the case of Location B, the damping controller has excellent performance in suppressing the interarea oscillations when a high droop coefficient is applied. For comparison, Figure 8(b) plots the time-domain responses under different values of K_{WT} when the WPP is placed at Location C. As shown in Figure 8(b), the damping controller deteriorates the dynamic stability of the system as K_{WT} increases. In addition, the damping effect of the PMSG auxiliary damping control when the WPP is located at the mass-weighted electrical centre is also fully investigated. As shown in Figure 8(c), the damping of this test basically remains the same when K_{WT} increases from 10 to 20, i.e., the effect of the damping controller is negligible.

The results mentioned above prove that the oscillation mode is sensitive to the droop coefficient except for the mass-weighted electrical centre. It also demonstrates that the location of the damping controller in Area 1 and Area 2 has different performances on LFO damping, which is consistent with the damping torque analysis in Section 4.2.

5.3. Impact of the Wind Power Penetration Level. In this section, the impact of the wind penetration was analysed by gradually displacing units of SG_1 and SG_2 with wind turbine generators. The eigenvalue computational results of Location B are shown in Table 3. It can be seen that, with the wind energy ratio varying from 30% to 50%, the damping ratio of interarea oscillation is increasing from 0.0201 to 0.0281. In addition, the interarea oscillation mode of the example WPP is given in the last row of Table 3, which shows that the mode moves to the left when the wind penetration increases.

Figure 9 plots the relationship between the wind penetration and the damping torque coefficient K_D when the WPP is located at Location B. As seen in Figure 9, the damping torque coefficient K_D increases with the increase of the wind penetration, and K_D is more intense in high wind penetration.

Table 4 shows the results of the interarea oscillation mode when the WPP is installed at Location C. It is shown that the damping ratio of the interarea mode improves with the increase in the wind energy contribution. The results of Figure 10 show that the damping torque coefficient of the studied system improves more with a high droop coefficient. Moreover, as displayed in Figure 10, the damping torque coefficient becomes positive when the wind penetration exceeds 54%. It can be attributed to the change in the operating condition of the system. The results in Figures 9 and 10 also confirm that the droop coefficient plays an important role in the effect of the wind energy ratio on the system damping.

To justify the findings in Tables 3 and 4, the time-domain simulations are presented in Figure 11. In Figure 11, the results of different wind energy ratios are compared when the WPP is installed at Location B and Location C, respectively. It can be found that high wind penetration has a beneficial impact on system damping. The simulations indicate that the PMSG auxiliary damping control is always helpful in improving the system damping as wind power penetration increases.

5.4. Impact of the Wind Speed. In practice, the wind speed is variable, and therefore, the PMSG output power also varies. To evaluate the effectiveness of the damping controller of PMSG, two scenarios of a sudden rise and a sudden drop in the wind speed are simulated by a nonlinear simulation. Figure 12 shows the rotor angle deviation between SG_1 and SG_2 for a given step wind speed when the WPP is installed at Location B. The wind speed steps up from 12 to 10 m/s at 1 s as depicted in Figure 12(a). As observed, the damping control is effective in suppressing the LFO with a higher droop. In addition, Figure 12(b) shows the simulation results when the wind speed changed from 12 to 14 m/s. It can be seen that the system is stable (positive damping) in the presence of the damping controller. The results show that the proposed damping controller provides superior performance against wind speed fluctuations as long as the WPP is installed in Area 1.

The effects of the proposed damping control are also investigated when the WPP is installed at Location B. As shown in Figure 13, the PMSG auxiliary damping control plays a negative role in damping the LFOs. In Figure 13(a), the system becomes unstable with negative damping when the wind speed suddenly drops from 12 to 10 m/s. As observed in Figure 13(b), a higher droop coefficient K_{WT} will deteriorate the modal damping when the WPP is installed in Area 2. Therefore, the LFO mode brings the system to instability under variable wind speed conditions as long as the WPP is installed in Area 2.

5.5. Results and Discussion. The damping coefficients derived by the DTA method reveal the impacts of PMSG location, the operation conditions, and the control parameters on the system damping characteristics. In conclusion, the following potentials for further investigation

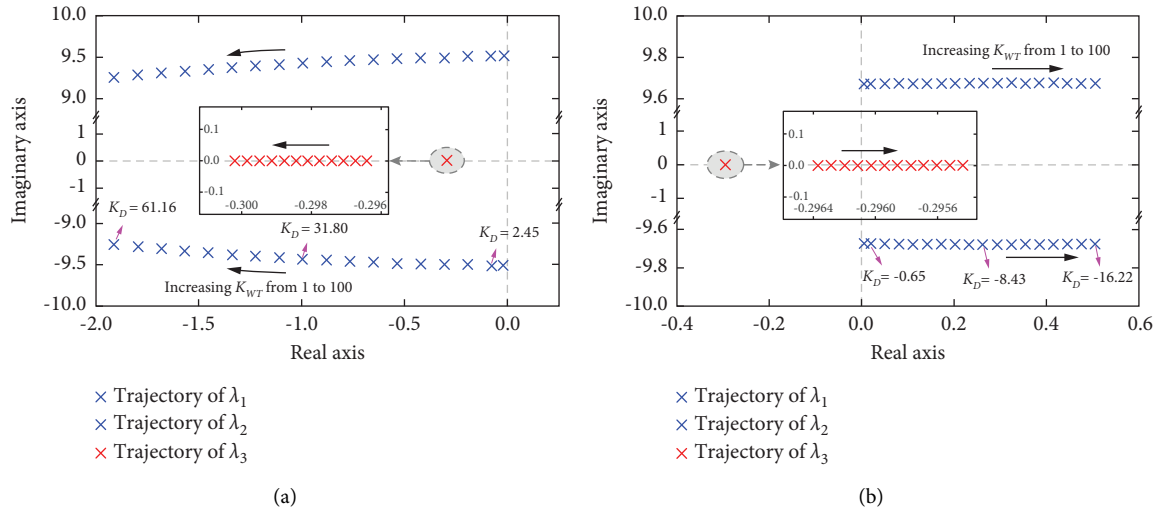

Figure 7: Eigenvalue trajectories as K_{WT} varies. (a) The WPP located at location B. (b) The WPP located at location C.

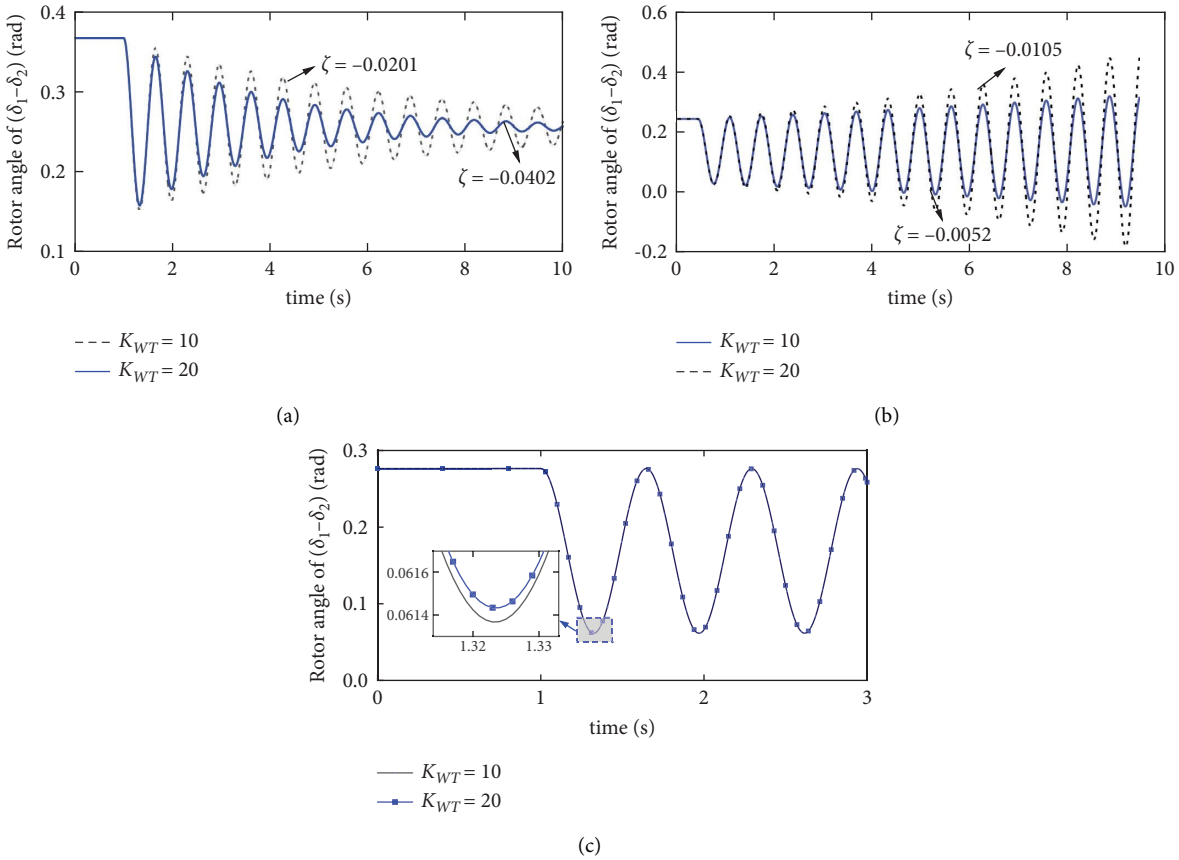

Figure 8: Simulation results of different K_{WT}. (a) The WPP located at location B. (b) The WPP located at location C. (c) The WPP located at the mass-weighted electrical centre.

and practical applications of the proposed method are demonstrated.

(1) The location of WPP is an important factor that influences the damping of LFOs. The effect of the proposed damping controller on system damping can be either positive or negative, depending on the location of WPP. It is found that the interarea mode is uncontrollable through power modulation as long as the WPP is installed at the mass-weighted electrical centre between the two areas. As for the two-area system integrated with a WPP, the location area

Table 3: Comparison of different wind energy ratios at location B ($K_{WT}=10$ and $l_w=0.167$).

The wind energy ratio (%)	30	40	50
Damping ratio	0.0201	0.0233	0.0281
K_D	6.12	6.87	7.93
Oscillation frequency (Hz)	1.51	1.47	1.40
Eigenvalue	-0.19 ± 9.51	$-0.21 \pm 9.22j$	$-0.25 \pm 8.80j$

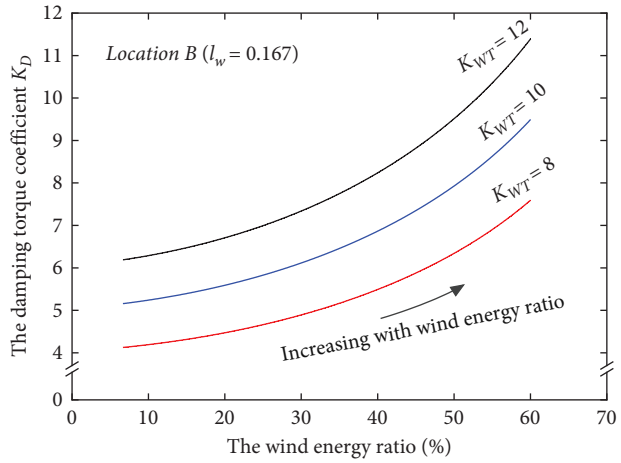

Figure 9: Damping torque coefficient K_D with varying wind energy ratios for different K_{WT} at location B.

Table 4: Comparison of different wind energy ratios at location C ($K_{WT}=10$ and $l_w=0.333$).

The wind energy ratio (%)	30	40	50
Damping ratio	−0.0052	−0.0036	−0.0012
K_D	−1.62	−1.08	−0.37
Oscillation frequency (Hz)	1.54	1.51	1.48
Eigenvalue	$0.05 \pm 9.67j$	$0.03 \pm 9.51j$	$0.01 \pm 9.28j$

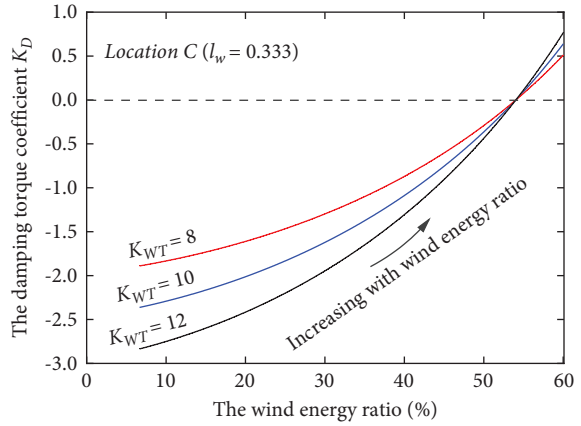

Figure 10: Damping torque coefficient K_D with varying wind energy ratios for different K_{WT} at location C.

is divided into an area of positive effect and a negative one by the mass-weighted electrical centre. The modulation will be more efficient at damping the LFO when the WPP is located in the positive effect area. On the contrary, the WT controller will deteriorate the LFO damping when the WPP is located in the negative effect area.

(2) Parameters of PMSG's control systems can be tuned to improve system damping. In this study, the explicit analytical relationships between the parameters of damping control and change in damping torque coefficient are derived. It can be concluded that the contribution of damping from the PMSG can be enhanced by increasing the droop coefficient when

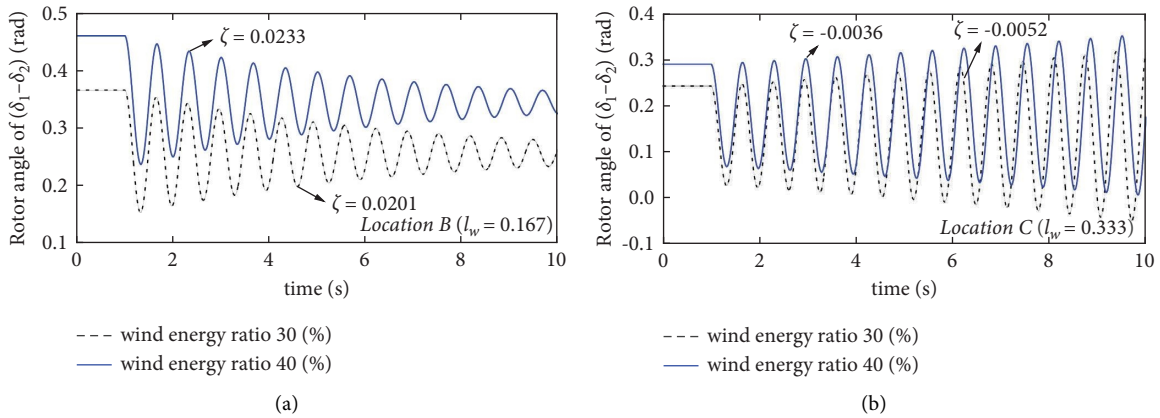

Figure 11: Simulation results of different wind energy ratios. (a) The WPP located at location B. (b) The WPP located at location C.

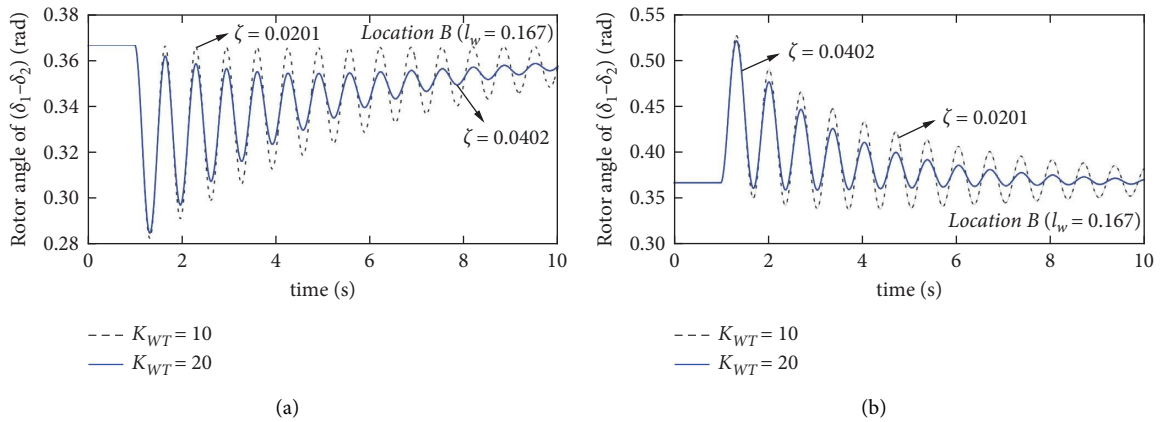

Figure 12: Simulation results of different K_{WT} at location B. (a) A sudden drop in the wind speed. (b) A sudden rise in the wind speed.

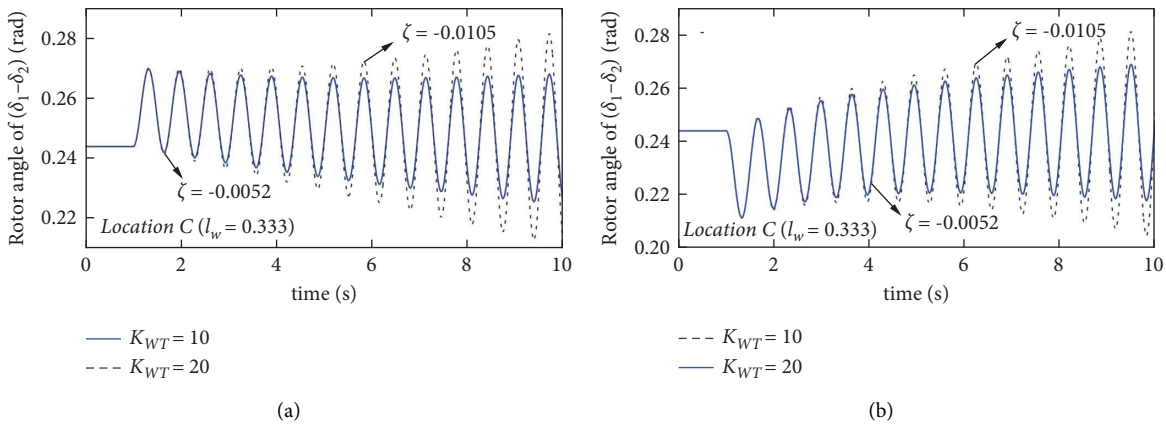

Figure 13: Simulation results of different K_{WT} at location C. (a) A sudden drop in the wind speed. (b) A sudden rise in the wind speed.

the WPP is installed in the area of positive effect. Conversely, a higher droop coefficient will deteriorate the damping level and aggravate the LFO when the WPP is installed in the area of negative effect. It is indicated that the parameters of the PMSG damping control should be adjusted according to the installation location of the WPP.

(3) The dynamic interactions introduced by the PMSG auxiliary damping controller are affected by the level of wind power penetration. It is found that, for the

same PMSG controller parameter settings, the variation of wind power penetration will alter the damping of LFO modes in the system. It is attributed to the change in the operating condition of the system. However, the PMSG auxiliary damping control proves to be beneficial to LFO damping as the wind power penetration increases.

It is shown that the damping control can provide considerable positive damping torque to effectively damp LFOs in power grids with proper control design. Particularly, using the damping torque analysis, the influences of the location of WPP, the control parameters, and the operation conditions are elaborately studied to provide design guidelines for better damping LFOs.

6. Conclusions

In this study, the DTA method is utilized to theoretically assess the impact of the WT supplementary damping controller on the LFOs. To enable the PMSG-based WT to provide damping support for interarea LFOs, an auxiliary damping controller is designed where the rotational speed signals are utilized for active power modulation. For analytical investigation, a reduced mathematical model of an interarea system oriented to the small-signal stability analysis is particularly developed in this study. Based on this, the equivalent damping torque coefficient is explicitly derived using the DTA method to examine the coupling effect between WT dynamics and synchronous generators. The effects of the WT control parameters (the droop coefficient) and the system operating condition (the WPP location) on the system damping properties are elaborately assessed, which gives guidelines on the control design for better damping enhancement. Case studies have been conducted to verify the proposed damping controller strategy and the theoretical analysis.

It is found that the damping effect of the PMSG controller on the LFOs can be positive or negative depending on the location of WPP. Also, it is interesting to find that the LFO mode is uncontrollable as long as the WPP is installed at the mass-weighted electrical centre between the two areas. Moreover, the parameters of the PMSG damping control can be adjusted to improve the system damping. And it is shown that the damping control is always beneficial in improving the system damping with the increase of wind power penetration. More discussions about interactions introduced by the damping control of the WT (i.e., the reactive power modulation) on LFOs will be fully discussed in our future works.

Abbreviations

D_i: Damping coefficient of SG_i
H_i: Inertia constant of SG_i
P_{Mi}: Mechanical power inputs of SG_i
P_{ei}: Active power outputs of SG_i
P_{L1}, P_{L2}: Local load
ω_i: Rotor speed of SG_i
δ_i: Rotor angle of SG_i
ω_s: Synchronous electrical angular velocity
X_i: Total reactance of the i_{th} transmission line
δ_3: Voltage phase at Bus 3
P_{e3}: Active power output from the wind farm
V_i: Bus voltage at node i
Δ: Incremental operator
a_1 and a_2: The defined variables
$\Delta\omega$: Rotational speed deviation between SG_1 and SG_2
$\Delta\delta$: Rotor angle deviation between SG_1 and SG_2
ω_n: Undamped natural mechanical mode frequency
ρ: Air density
R: Rotor blade radius
k: Gear ratio of the gearbox
λ: Tip speed ratio
C_p: Maximum power coefficient
ω_t: Generator rotational speed of WPP
P_{WT}: Generated active power of WPP
P_{MPPT}: Power reference determined by the MPPT algorithm
H_t: Inertia time constant of the PMSG
ω_{sys}: System rotational speed
ω_{nom}: Nominal rotational speed
K_{WT}: Droop coefficient
ΔP_{droop}: Output of the droop control loop
$F(s)$: Electrical torque
T_J: Equivalent inertia constant
K_S: Synchronizing torque coefficient
K_D: Damping torque coefficient
X_{li}: Reactance of the ith transmission line
l_w: The relative distance from SG_1
X: Total reactance of the transmission lines
X_{Ti}: Reactance of the ith transformer
SG: Synchronous generator
WT: Wind turbine
PMSG: Permanent magnet synchronous generator
LFO: Low-frequency oscillation
DTA: Damping torque analysis
MA: Modal analysis
DFIG: Doubly fed induction generator
PSS: Power system stabiliser
RSC: Rotor-side converter
GSC: Grid-side converter
WPP: Wind power plant
MPPT: Maximum power point tracking
WACS: Wide area control systems
SMIB: Single-machine infinite bus
Superscripts "(0)": Steady-state value of variables.

Data Availability

The data that support the findings of this study can be obtained from the corresponding author upon reasonable request.

Conflicts of Interest

The authors declare that they have no known conflicts of interest.

Acknowledgments

This work was supported by the National Natural Science Foundation of China, under Grant 52277122.

Supplementary Materials

The parameters used in the simulation study are given in Tables S1 and S2. Table S1 shows the basic parameters of the two-area system. Table S2 shows the parameters of the PMSG wind turbine. (*Supplementary Materials*)

References

[1] P. Kundur, *Power System Stability and Control*, McGraw-Hill, New York, NY, USA, 1994.

[2] H. Ahmadi and H. Ghasemi, "Maximum penetration level of wind generation considering power system security limits," *IET Generation, Transmission & Distribution*, vol. 6, no. 11, pp. 1164–1170, 2012.

[3] H. Abubakr, J. C. Vasquez, K. Mahmoud, M. M. F. Darwish, and J. M. Guerrero, "Comprehensive review on renewable energy sources in Egypt—current status, grid codes and future vision," *IEEE Access*, vol. 10, pp. 4081–4101, 2022.

[4] M. Elsisi, M.-Q. Tran, K. Mahmoud, M. Lehtonen, and M. M. F. Darwish, "Robust design of ANFIS-based blade pitch controller for wind energy conversion systems against wind speed fluctuations," *IEEE Access*, vol. 9, pp. 37894–37904, 2021.

[5] X. Guo, D. Zhu, J. Hu, X. Zou, Y. Kang, and J. M. Guerrero, "Inertial PLL of grid-connected converter for fast frequency support," *CSEE Journal of Power and Energy Systems*, 2022.

[6] X. Yuan, Z. Du, Y. Li et al., "Novel cascading scheme of VSC-HVDC with DC voltage synchronisation control for system frequency support," *IET Generation, Transmission & Distribution*, vol. 15, no. 24, pp. 3502–3519, 2021.

[7] E. Hagstrom, I. Norheim, and K. Uhlen, "Large-scale wind power integration in Norway and impact on damping in the Nordic grid," *Wind Energy*, vol. 8, no. 3, pp. 375–384, 2005.

[8] H. Abubakr, J. M. Guerrero, J. C. Vasquez et al., "Adaptive LFC incorporating modified virtual rotor to regulate frequency and tie-line power flow in multi-area microgrids," *IEEE Access*, vol. 10, pp. 33248–33268, 2022.

[9] M. N. Ali, M. Soliman, K. Mahmoud, J. M. Guerrero, M. Lehtonen, and M. M. F. Darwish, "Resilient design of robust multi-objectives PID controllers for automatic voltage regulators: d-decomposition approach," *IEEE Access*, vol. 9, pp. 106589–106605, 2021.

[10] M. Klein, G. J. Rogers, and P. Kundur, "A fundamental study of inter-area oscillations in power systems," *IEEE Transactions on Power Systems*, vol. 6, no. 3, pp. 914–921, 1991.

[11] K. Sebaa, Y. Zhou, Y. Li, A. Gelen, and H. Nouri, "Low-frequency oscillation damping control for large-scale power system with simplified virtual synchronous machine," *Journal of Modern Power Systems and Clean Energy*, vol. 9, no. 6, pp. 1424–1435, 2021.

[12] M. Edrah, X. Zhao, W. Hung et al., "Electromechanical interactions of full scale converter wind turbine with power oscillation damping and inertia control," *International Journal of Electrical Power & Energy Systems*, vol. 135, Article ID 107522, 2022.

[13] C. Zhang, D. Ke, Y. Sun, C. Y. Chung, J. Xu, and F. Shen, "Coordinated supplementary damping control of DFIG and PSS to suppress inter-area oscillations with optimally controlled plant dynamics," in *Proceedings of the 2018 IEEE Power & Energy Society General Meeting (PESGM)*, p. 1, Portland, OR, USA, April 2018.

[14] C. Du, Y. Han, and S. Li, "Continuous twisting damping control of DFIG-based wind farm to improve interarea oscillation damping," in *Proceedings of the 2021 China Automation Congress (CAC)*, pp. 5432–5437, Beijing, China, March 2021.

[15] X. Shi, Y. Cao, M. Shahidehpour, Y. Li, X. Wu, and Z. Li, "Data-driven wide-area model-free adaptive damping control with communication delays for wind farm," *IEEE Transactions on Smart Grid*, vol. 11, no. 6, pp. 5062–5071, 2020.

[16] M. Basu, J. Kim, R. M. Nelms, and E. Muljadi, "Interarea-oscillation damping with dual power oscillation damping controller of a utility-scale wind power plant," in *Proceedings of the 2021 3rd International Conference on High Voltage Engineering and Power Systems (ICHVEPS)*, pp. 581–585, Bandung, Indonesia, October 2021.

[17] N. Gurung, R. Bhattarai, and S. Kamalasadan, "Optimal oscillation damping controller design for large-scale wind integrated power grid," *IEEE Transactions on Industry Applications*, vol. 56, no. 4, pp. 1–4235, 2020.

[18] D. Gautam, V. Vittal, R. Ayyanar, and T. Harbour, "Supplementary control for damping power oscillations due to increased penetration of doubly fed induction generators in large power systems," in *Proceedings of the IEEE/PES Power Systems Conference and Exposition (PSCE 2011)*, pp. 1–6, Phoenix, AZ, USA, March 2011.

[19] M. Edrah, K. L. Lo, and O. A. Lara, "Impacts of high penetration of DFIG wind turbines on rotor angle stability of power systems," *IEEE Transactions on Sustainable Energy*, vol. 6, no. 3, pp. 759–766, 2015.

[20] T. Knüppel, J. N. Nielsen, K. H. Jensen, A. Dixon, and J. Ostergaard, "Power oscillation damping capabilities of wind power plant with full converter wind turbines considering its distributed and modular characteristics," *IET Renewable Power Generation*, vol. 7, no. 5, pp. 431–442, 2013.

[21] T. Wang, M. Jin, Y. Li, J. Wang, Z. Wang, and S. Huang, "Adaptive damping control scheme for wind grid-connected power systems with virtual inertia control," *IEEE Transactions on Power Systems*, vol. 37, no. 5, pp. 3902–3912, 2022.

[22] K. Liao, Z. He, Y. Xu, G. Chen, Z. Y. Dong, and K. P. Wong, "A sliding mode based damping control of DFIG for interarea power oscillations," *IEEE Transactions on Sustainable Energy*, vol. 8, no. 1, pp. 258–267, 2017.

[23] M. Edrah, K. L. Lo, and O. A. Lara, "Reactive power control of DFIG wind turbines for power oscillation damping under a wide range of operating conditions," *IET Generation, Transmission & Distribution*, vol. 10, no. 15, pp. 3777–3785, 2016.

[24] J. L. D. García, O. G. Bellmunt, F. D. Bianchi, and A. Sumper, "Power oscillation damping supported by wind power: a review," *Renewable and Sustainable Energy Reviews*, vol. 16, no. 7, pp. 4994–5006, 2012.

[25] Y. J. Isbeih, M. S. El Moursi, W. Xiao, and E. Saadany, "Mixed-sensitivity robust control design for damping low-frequency oscillations with DFIG wind power generation," *IET Generation, Transmission & Distribution*, vol. 13, no. 19, pp. 4274–4286, 2019.

[26] M. Mokhtari and F. Aminifar, "Toward wide-area oscillation control through doubly-fed induction generator wind farms," *IEEE Transactions on Power Systems*, vol. 29, no. 6, pp. 2985–2992, 2014.

[27] S. Li, H. Zhang, Y. Yan, and J. Ren, "Parameter optimization to power oscillation damper (POD) considering its impact on the DFIG," *IEEE Transactions on Power Systems*, vol. 37, no. 2, pp. 1508–1518, 2022.

[28] L. Fan, H. Yin, and Z. Miao, "On active/reactive power modulation of DFIG-based wind generation for interarea oscillation damping," *IEEE Transactions on Energy Conversion*, vol. 26, no. 2, pp. 513–521, 2011.

[29] M. Ramirez, G. Calderon, and R. Castellanos, "Effect of PODCs for DFIG based wind farms in the inter-area and torsional oscillation damping," *IEEE Latin America Transactions*, vol. 14, no. 8, pp. 3648–3654, 2016.

[30] G. Tsourakis, B. M. Nomikos, and C. D. Vournas, "Contribution of doubly fed wind generators to oscillation damping," *IEEE Transactions on Energy Conversion*, vol. 24, no. 3, pp. 783–791, 2009.

[31] W. Du, X. Chen, and H. F. Wang, "Impact of dynamic interactions introduced by the DFIGs on power system electromechanical oscillation modes," *IEEE Transactions on Power Systems*, vol. 32, no. 6, pp. 4954–4967, 2017.

[32] M. Baruwa and M. Fazeli, "Impact of virtual synchronous machines on low-frequency oscillations in power systems," *IEEE Transactions on Power Systems*, vol. 36, no. 3, pp. 1934–1946, 2021.

[33] J. Morató, T. Knüppel, and J. Østergaard, "Residue-based evaluation of the use of wind power plants with full converter wind turbines for power oscillation damping control," *IEEE Transactions on Sustainable Energy*, vol. 5, no. 1, pp. 82–89, 2014.

[34] M. J. Morshed and A. Fekih, "A probabilistic robust coordinated approach to stabilize power oscillations in DFIG-based power systems," *IEEE Transactions on Industrial Informatics*, vol. 15, no. 10, pp. 5599–5612, 2019.

[35] H. P. Painemal, Y. Wang, and H. S. Saravia, "On inertia distribution, inter-area oscillations and location of electronically-interfaced resources," *IEEE Transactions on Power Systems*, vol. 33, no. 1, pp. 995–1003, 2018.

[36] F. P. Demello and C. Concordia, "Concepts of synchronous machine stability as affected by excitation control," *IEEE Transactions on Power Apparatus and Systems*, vol. 88, no. 4, pp. 316–329, 1969.

[37] D. Obradović, M. Oluić, R. Eriksson, and M. Ghandhari, "Supplementary power control of an HVDC system and its impact on electromechanical dynamics," *IEEE Transactions on Power Systems*, vol. 36, no. 5, pp. 4599–4610, 2021.

[38] W. Du, J. Bi, C. Lv, and T. Littler, "Damping torque analysis of power systems with DFIGs for wind power generation," *IET Renewable Power Generation*, vol. 11, no. 1, pp. 10–19, 2017.

[39] T. Smed and G. Andersson, "Utilizing HVDC to damp power oscillations," *IEEE Transactions on Power Delivery*, vol. 8, no. 2, pp. 620–627, 1993.

[40] L. Harnefors, N. Johansson, L. Zhang, and B. Berggren, "Interarea oscillation damping using active-power modulation of multiterminal HVDC transmissions," *IEEE Transactions on Power Systems*, vol. 29, no. 5, pp. 2529–2538, 2014.

[41] W. Du, J. Bi, J. Cao, and H. F. Wang, "A method to examine the impact of grid connection of the DFIGs on power system electromechanical oscillation modes," *IEEE Transactions on Power Systems*, vol. 31, no. 5, pp. 3775–3784, 2016.

[42] W. Du, Q. Fu, and H. Wang, "Damping torque analysis of dc voltage stability of an MTDC network for the wind power delivery," *IEEE Transactions on Power Delivery*, vol. 35, no. 1, pp. 324–338, 2020.

[43] Q. Fu, W. Du, H. F. Wang, and B. Ren, "Analysis of small-signal power oscillations in MTDC power transmission system," *IEEE Transactions on Power Systems*, vol. 36, no. 4, pp. 3248–3259, 2021.